Available online at www.sciencedirect.com
SCIENCE DIRECT
ELSEVIER
Tectonophysics 418 (2006) 235–254
TECTONOPHYSICS
www.elsevier.com/locate/tecto

Kinematics and $^{40}Ar/^{39}Ar$ geochronology of the Gaoligong and Chongshan shear systems, western Yunnan, China: Implications for early Oligocene tectonic extrusion of SE Asia

Yuejun Wang [a,*], Weiming Fan [a], Yanhua Zhang [b], Touping Peng [a], Xinyue Chen [a], Yigang Xu [a]

[a] *Key Laboratory of Isotope Geochronology and Geochemistry, Guangzhou Institute of Geochemistry, Chinese Academy of Sciences, Guangzhou 510640, PR China*
[b] *CSIRO Exploration and Mining, PO Box 1130, Bentley, WA 6102, Australia*

Received 20 August 2005; received in revised form 13 February 2006; accepted 15 February 2006
Available online 5 April 2006

Abstract

The Gaoligong and Chongshan shear systems (GLSS and CSSS) in western Yunnan, China, have similar tectonic significance to the Ailaoshan–Red River shear system (ASRRSS) during the Cenozoic tectonic development of the southeastern Tibetan syntaxis. To better understand their kinematics and the Cenozoic tectonic evolution of SE Asia, this paper presents new kinematic and $^{40}Ar/^{39}Ar$ geochronological data for these shear systems. All the structural and microstructural evidence indicate that the GLSS is a dextral strike-slip shear system while the CSSS is a sinistral strike-slip shear system, and both were developed under amphibolite- to greenschist-grade conditions. The $^{40}Ar/^{39}Ar$ dating of synkinematic minerals revealed that the strike-slip shearing on the GLSS and CSSS at least began at ~32 Ma, possibly coeval with the onset of other major shear systems in SE Asia. The late-stage shearing on the GLSS and CSSS is dated at ~27–29 Ma by the biotite $^{40}Ar/^{39}Ar$ ages, consistent with that of the Wang Chao shear zone (WCSZ), but ~10 Ma earlier than that of the ASRRSS. The dextral Gaoligong shear zone within the GLSS may have separated the India plate from the Indochina Block during early Oligocene. Combined with other data in western Yunnan, we propose that the Baoshan/Southern Indochina Block escaped faster southeastward along the CSSS to the east and the GLSS to the west than the Northern Indochina Block along the ASRRSS, accompanying with the obliquely northward motion of the India plate during early Oligocene (28–36 Ma). During 28–17 Ma, the Northern Indochina Block was rotationally extruded along the ASRRSS relative to the South China Block as a result of continuously impinging of the India plate.

Keywords: Kinematics; $^{40}Ar/^{39}Ar$ geochronology; Tectonic extrusion; Early Oligocene; Gaoligong and Chongshan shear systems; Western Yunnan

1. Introduction

The Cenozoic tectonic evolution of the southeastern Tibetan Plateau associated with the indentation of India plate has been long debated. Several distinct hypotheses have been postulated over the past 30 years. Tapponnier

* Corresponding author. Current address: Guangzhou Institute of Geochemistry, Chinese Academy of Sciences, PO Box 1131, Guangzhou 510640, People's Republic of China. Tel.: +86 20 85290527; fax: +86 20 85290708.
E-mail address: yjwang@gig.ac.cn (Y. Wang).

0040-1951/$ - see front matter © 2006 Elsevier B.V. All rights reserved.
doi:10.1016/j.tecto.2006.02.005

et al. (1982, 1986), and Replumaz and Tapponnier (2003) suggested that the northward movement of the India plate relative to the Eurasia plate caused southeastward extrusion of the Indochina Block away from the convergent front, possibly with internal contractional deformation. The extrusion was also thought to be responsible for the opening of the South China Sea (e.g., Tapponnier et al., 1982; Briais et al., 1983; Pelzer and Tapponnier, 1988). In this hypothesis, large-scale strike-slip faults were predicated to dominate the Cenozoic tectonic evolution of SE Asia (Leloup et al., 1993, 1995; Lacassin et al., 1997). In contrast, England and Houseman (1989), and Houseman and England (1993) postulated that contractional structures and crustal thickening extensively developed within the Tibetan Plateau, with only minor eastward extrusion of crustal materials (England and Molnar, 1990), as also suggested by Meyer et al. (1998) and Cattin and Avouac (2000). Wang and Burchfiel (1997, 2000) considered that the continental materials between the Ailaoshan–Red River shear system (ASRRSS) and southeastern Tibetan syntaxis were strongly deformed internally, and the clockwise rotation of the Indochina Block might have been important.

A key issue of debate among these hypotheses is whether the crustal deformation related to the

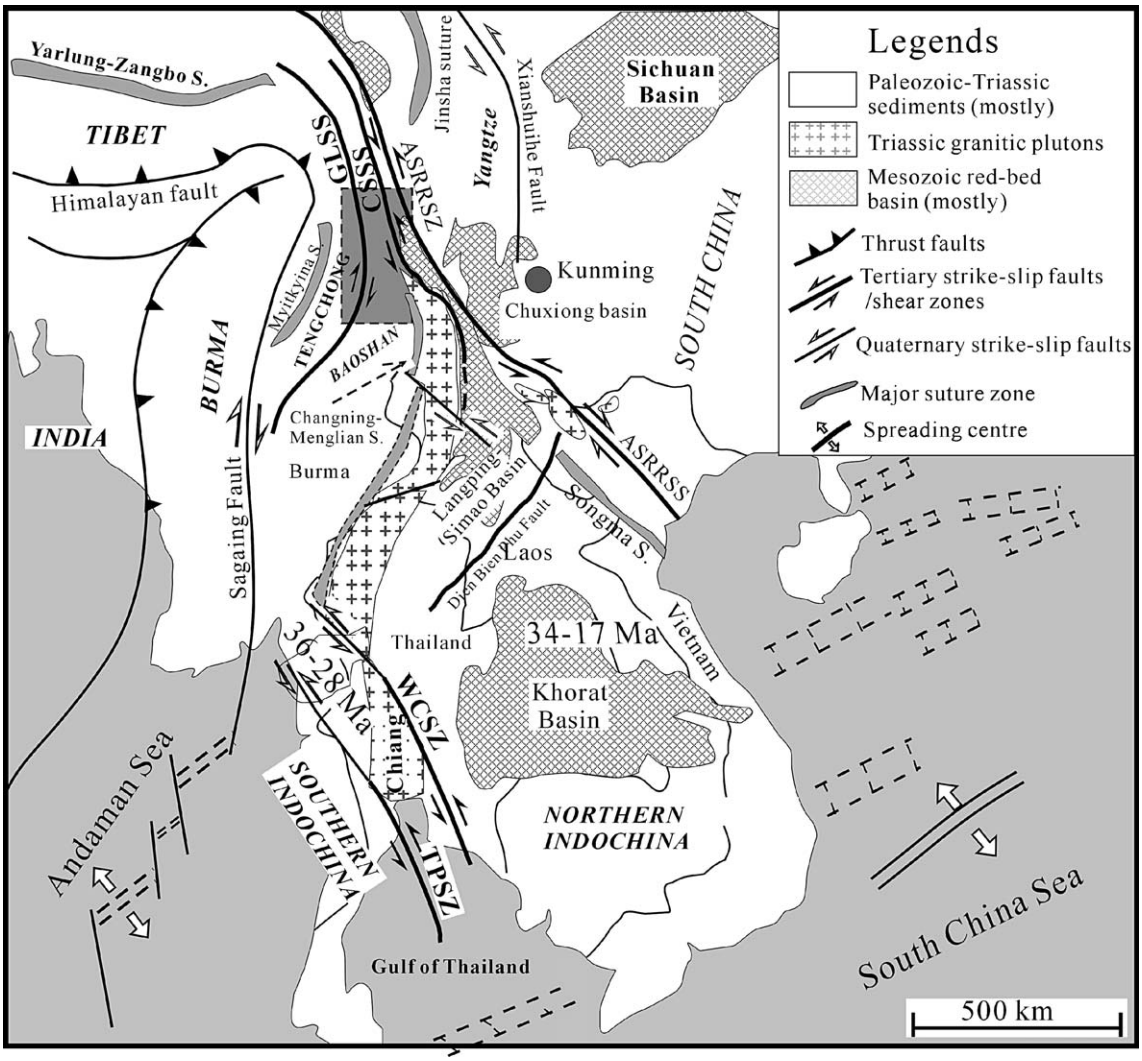

Fig. 1. Tectonic sketch map of SE Asia showing major faults/shear systems (after Gilley et al., 2003). ASRRSS: the Ailaoshan–Red River shear system; GLSS: the Gaoligong shear system; CSSS: the Chongshan shear system; WCSZ: the Wang Chao shear zone; TPSZ: the Three Pagodas shear zone.

convergence between the India and Eurasia plates was accommodated by crustal shortening, or by lateral extrusion outward from the Plateau (e.g., Dewey et al., 1989; Wang and Burchfiel, 1997). To address this issue and test different hypotheses, it is vital to determine the kinematics and deformational timing of the major shear systems in the southeastern Tibetan syntaxis, such as the ASRRSS, Chongshan shear system (CSSS), Gaoligong shear system (GLSS), Wang Chao shear zone (WCSZ) and Three Pagodas shear zone (TPSZ) as shown in Fig. 1. The structural and geochronological studies of some of these shear systems (e.g., ASRRSS, WCSZ and Jiali shear zone) have been systematically carried out (Leloup and Kienast, 1993; Leloup et al., 1993, 1995; Lacassin et al., 1997; Wang et al., 1998, 2000; Leloup et al., 2001; Lee et al., 2003). However, little attention has been paid to the kinematics and geochronology of the GLSS and CSSS, as well as the influence of the India–Eurasian collision on these shear systems (Wang and Burchfiel, 1997; Ji et al., 2000). There is also little knowledge for the following questions: (1) are these major shear systems dominated by strike-slip or contraction? (2) is their formation associated with the India–Eurasia collision? and (3) are they contemporaneous with the ASRRSS? Addressing these questions is crucial to achieving a better understanding of the roles of these shear systems during the Cenozoic tectonic evolution of SE Asia.

To answer these questions, we have carried out a kinematic study of the GLSS and CSSS in the Nujiang–Lancangjiang–Jinshajiang area (also called the San-Jiang area in Chinese literature) in western Yunnan, China, combined with $^{40}Ar/^{39}Ar$ geochronological analyses of synkinematic minerals from these shear systems. In this paper we present our new data and describe the deformational patterns surrounding the southeastern Tibetan syntaxis, and then discuss the relationship between the Cenozoic tectonic evolution of SE Asia and the India–Eurasia collision.

2. Geological overview of the study area

The San-Jiang area is an important region in the southeastern Tibetan syntaxis, with strong Cenozoic deformation and structural overprinting. The area is bounded by the ASRRSS to the northeast and the Sagaing fault (the present-day western boundary of the Indochina Block, e.g., Replumaz and Tapponnier, 2003) to the southwest, and has a wedge-shaped geometry with its narrower northwestern end adjoining the Himalaya syntaxis and its broader side facing the southeast (Fig. 1). In the region, from west to east, three tectonic units (the Tengchong block, Baoshan block and Lanping–Simao fold belt) are separated by the GLSS and CSSS, respectively (Fig. 2; Wang and Burchfiel, 1997; Ji et al., 2000).

The Tengchong block, the northern continuation of the Mogok metamorphic belt (Mitchell, 1993), is located in the westernmost Yunnan and extends southwestward into Burma (Fig. 2). It is mainly composed of pre-Mesozoic high-grade metamorphic rocks, Mesozoic–Tertiary granites and Quaternary volcanic–sedimentary strata (Liu et al., 1993). The block has been considered as part of Gondwana during the late Paleozoic, which was accreted to Eurasia during the late Mesozoic (Wang, 1983; Morley et al., 2001). The western boundary of the Tengchong block is defined by the dextral Sagaing fault with a total displacement of ~700 km, which was not active before middle Miocene (~15 Ma) and was related to the closure of the Andaman Sea basin (Morley et al., 2001; Replumaz and Tapponnier, 2003). Its eastern boundary likely coincides with the Gaoligong shear zone in the GLSS (Figs. 1 and 2).

The Baoshan block is bounded by the Gaoligong shear zone to the west and the Chongshan shear zone to the east (Fig. 2). This block displays wedge geometry with its narrower part in the north linking to the southeastern Tibetan syntaxis and its wider part in the south extending into Burma and northwestern Thailand. The block is mainly composed of pre-Mesozoic metamorphic rocks, Late Triassic granites, arc-related volcanic–sedimentary sequences and minor Cenozoic strata. It is considered that the block was merged with the Yangtze Block by the late Paleozoic subduction/collision along the Changning–Menglian suture (Figs. 1 and 2; Zhong, 1998).

The Lanping–Simao fold belt is bounded by the CSSS and ASRRSS, and extends southeastward into Vietnam and Laos. This belt contains the Proterozoic basement and Paleozoic marine strata that might be similar to those of the Yangtze Block. Triassic volcanics and molasse sediments are mainly exposed along the southwestern margin of the belt (Zhong, 1998; Peng et al., 2006). Rocks from Jurassic upwards are composed of continental redbeds (over 7 km thick), which rest unconformably on pre-Mesozoic strata. The pre-Miocene rocks exposed in the fold belt exhibit consistent deformation structures. The most significant structural feature is represented by three first-order arcuate fold-thrust belts: the Lanping and Simao belts that are convex to the southwest, and the Wuliangshan belt that is convex to the northeast (Fig. 2; BGMRYP, 1990; Wang and Burchfiel, 1997, 2000).

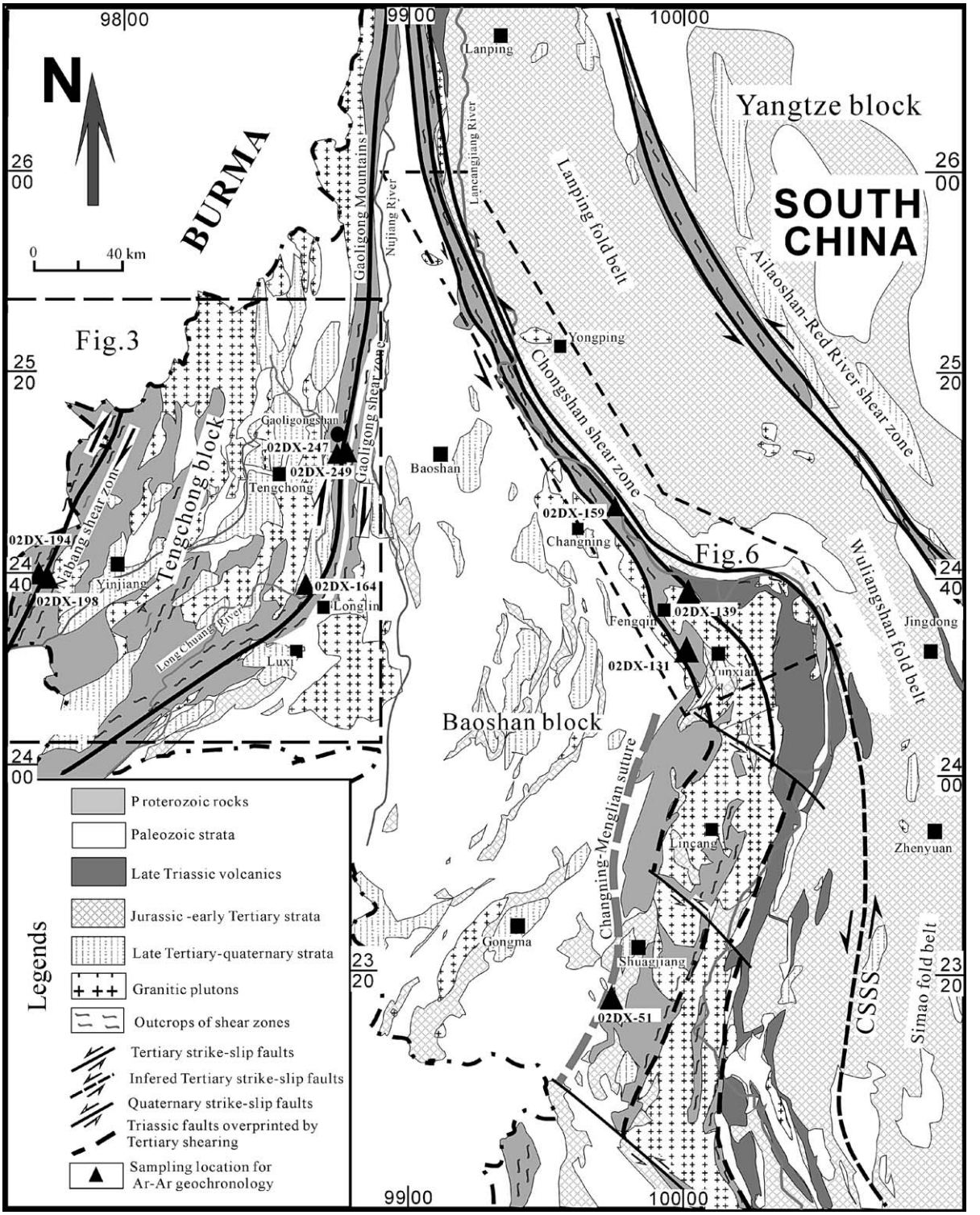

Fig. 2. Geological map of western Yunnan, drawn from the 1:1 000 000 scale geological map of western Yunnan Province (BGMRYP, 1990).

3. Kinematic natures of the shear systems

3.1. Gaoligong shear system

The Gaoligong shear system (GLSS) extends southward from the southeastern Tibetan syntaxis to the Longling–Yinjiang areas and then changes into a NE trend to meet the Sagaing fault (see Figs. 1 and 2). The GLSS consists of a series of N- to NE-trending high strain shear zones that are meter- to kilometer-scale wide and several hundreds of kilometers long (BGMRYP, 1990). The most important high strain zones include the Gaoligong and Nabang shear zones (Fig. 3).

The 500 m- to 6 km-wide Gaoligong shear zone exposes along the Gaoligong Mountains west of the Nujiang valley, and forms the boundary between the Tengchong and Baoshan blocks (Wang and Burchfiel, 1997; Zhong, 1998; Ji et al., 2000). Replumaz and Tapponnier (2003) proposed that it is a dextral shear zone that separated the Lhasa from Indochina Block prior to 15 Ma. It extends northward into the southeastern Tibetan syntaxis where it may join with the Jiali shear zone. Its southwestern segment is probably linked with the Sagaing fault. Mylonitic granite and the Proterozoic Gaoligong Group are mainly exposed on the western side of the Gaoligong shear zone, and the eastern side of the shear zone is dominated by the Paleozoic Gongyanghe Group (Fig. 3).

Mylonitic rocks in the northern segment of the Gaoligong shear zone (e.g., the Gaoligong, Dahaoping and Pumaoshao areas) contain a northerly trending foliation with a subhorizontally (2–12°) plunging mineral lineation. The foliation dips steeply (>55°) to the west in the eastern part and to the east in the western part of the shear zone, forming an inwardly dipping foliation pattern (see Fig. 3A–B and profile I–I′). Well developed S–C fabrics (Fig. 4a), asymmetric feldspar porphyroclasts (Fig. 4b) and mica flakes (Fig. 5a) indicate a dextral shear sense. The southern segment of the Gaoligong shear zone curves into a NE–SW orientation near the Longlin County (see Fig. 2). In this segment, the mylonitic foliation strikes 030–050° and dips 45–70° to the NW, and the stretching lineation generally plunges 5–25° to the SW (Fig. 3C–D). Asymmetric feldspar porphyroclasts with strongly attenuated tails (Fig. 4c), S–C fabrics (Fig. 5b) and C′-type shear band cleavage in granitic gneiss and schist, and Z-shaped asymmetric folds provide clear evidence of the dextral shear.

Geology of the Nabang shear zone is poorly known. The shear zone was not shown in the previously published geological map, and was only described by Zhong (1998) and Ji et al. (2000). We herein merge the shear zone into the GLSS due to its similar structural features (e.g., trending) to the Gaoligong shear zone. It extends over 100 km along the border of Burma and China, and its exposed width varies from 200 m to 5 km (Ji et al., 2000; Fig. 2). The main rock-types exposed in this shear zone are mylonitic granitoids, gneiss, micaschist, marble, amphibolite and minor mafic enclaves. These deformed rocks commonly have metamorphic mineral assemblages that are composed of plagioclase, quartz, biotite, chlorite and opaque minerals in gneiss, and hornblende and plagioclase in amphibolite, similar to those of the Gaoligong shear zone (Table 1). They are characterized by the development of S and S–L tectonic fabrics.

In the Nabang shear zone (e.g., the Tongbiguan–Nabang and Sudian areas), the mylonitic rocks contain stretching lineations plunging 3–25° to the NNE (0–030°) on the well-developed, steeply ENE-dipping foliations wrapping around asymmetric feldspar porphyroclasts (Fig. 3E–F and profile II–II′). In the shear zone, the overturned and recumbent folds are locally developed, mostly having thickened hinges and thinned limbs, and having axes plunging to the ENE. The banded mylonitic rocks are usually folded into upright and recumbent folds with the hinges parallel to stretching lineations. Well-developed S–C fabrics, mica flakes, abundant asymmetric porphyroclasts of feldspar and Z-shaped asymmetric folds of gneissic banding are commonly present (Fig. 4d). These structures consistently indicate a dextral movement in the shear zone.

3.2. Chongshan shear system

The Chongshan shear system (CSSS) is interpreted by Wang and Burchfiel (1997, 2000) as a sinistral Cenozoic fault system with similar tectonic importance to the ASRRSS during the development of the southeastern Tibetan syntaxis, but its general geology is still poorly known. The exposed CSSS can be traced northward to the Himalaya syntaxis and southward to the south of Yunxian, and exhibits many lithological similarities to the ASRRSS (Figs. 2 and 6; BGMRYP, 1990). The CSSS consists of a northerly trending northern segment along the eastern Chongshan Mountains, a NW–SE trending middle segment along the Lancangjiang valley (Chaojian–Yunxian areas), and an unknown southern segment that trends possibly either along Lincang granitic pluton or Simao fold belt (BGMRYP, 1990). In this study, we focus on the high strain zone in the middle segment, which is herein named the Chongshan shear zone (Fig. 6).

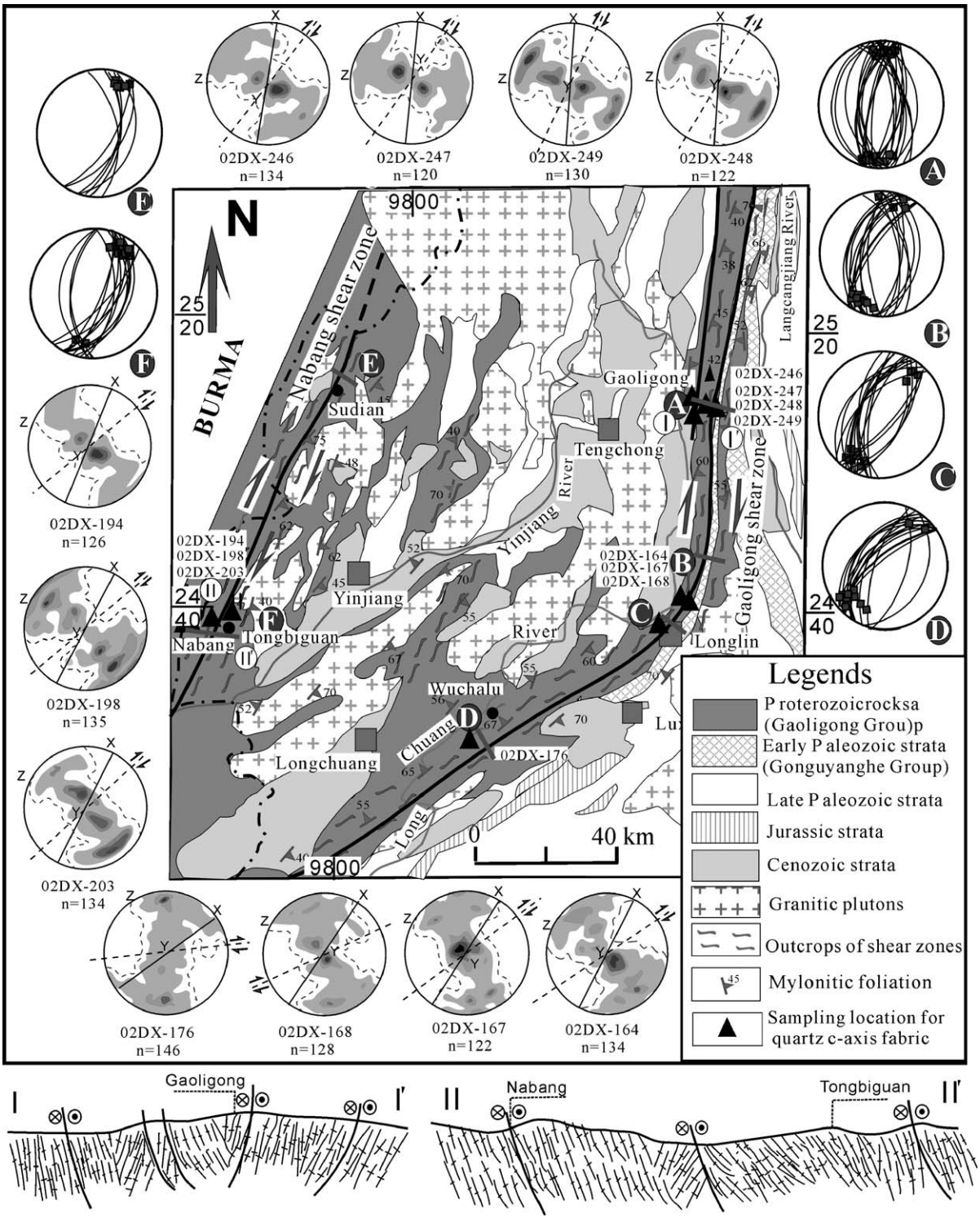

Fig. 3. Geological map (modified from BGMRYP, 1990) of the Gaoligong shear system (GLSS), showing stereoplots (A–F) of mylonitic foliations and stretching lineations (small filled squares) and illustrations of quartz *c*-axis preferred orientations (lower hemisphere, equal area, 1%, 4%, 7% and 10% of contour intervals) for representative mylonitic samples. See Table 1 for detailed sample locations. I–I′ and II–II′ are the sections of the Nabang shear zone across Tongbiguan–Nabang range and Gaoligong shear zones across Gaoligong Mountains within the GLSS, respectively.

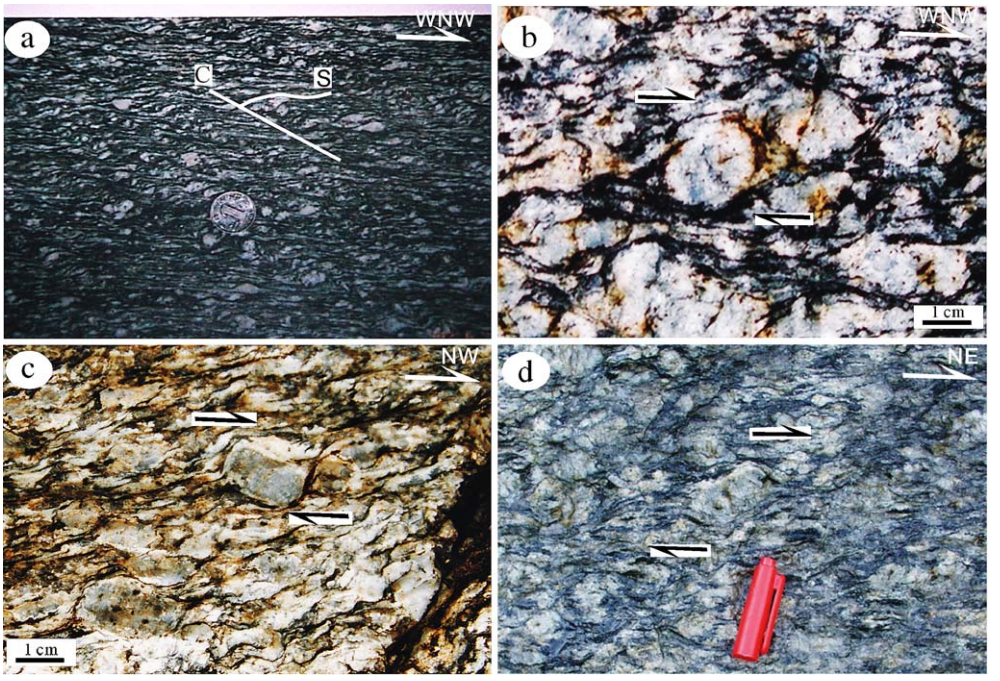

Fig. 4. Photographs showing dextral shear sense for the GLSS. (a) S–C fabrics in granitic gneiss (Dahaoping, Gaoligong Mountains). (b) Rolling structures in foliated granite (Pumanshao, Gaoligong Mountains) in the northern segment of the Gaoligong shear zone. (c) Rolling structures in foliated granite (Tianba, Longlin) and (d) asymmetric porphyroclasts in foliated granitic gneiss at site 02DX-203. Panels (b) and (c) are from polished thin sections perpendicular to foliation and parallel to stretching lineation (view from above).

The NNW-trending Chongshan shear zone has a width of 400–2000 m and a length of more than 200 km and generally dips moderately to steeply toward the northeast (BGMRYP, 1990; Fig. 6). It is mainly developed within the Chongshan Group, Triassic granites and Mesozoic sequences or along the unconformity between the Chongshan Group and Paleozoic/Mesozoic strata, roughly separating the Triassic arc-related sequence from the Mesozoic redbeds of the Lanping fold belt. In the area north of Yunxian, the shear zone is best exposed in foliated granite and gneiss. South of Yunxian, the shear zone is sinistrally truncated by NW-trending faults (BGMRYP, 1990, Fig. 2) and its southward continuation is poorly known.

To the north of Chaojian, mylonites within the shear zone contain a northerly trending foliation that dips steeply to the east, with a subhorizontal mineral lineation (Fig. 6A). A northerly trending gneissic banding is parallel to numerous pegmatite veins, some of which are strongly boudinaged. In the Chaojian–Changjie area, a northerly trending steep foliation curves into a NW trend, where it commonly contains a gently plunging mineral lineation (Fig. 6B). To the southeast (e.g., at Mangshuijie and Xiaowan), a pervasive, NW-trending foliation dips moderately toward the northeast, with a subhorizontal to shallowly plunging (5–25°) mineral lineation to the SE (120–160°, Figs. 6C–E). In the Pingba–Yangtouyan area, a NW-dipping steep foliation with a shallowly plunging lineation is commonly present (Fig. 6F). Within the shear zone, a sinistral shear sense is commonly indicated by asymmetric feldspar porphyroclasts and quartzo-feldspathic aggregates, S–C fabrics and the geometry of small-scale restraining jogs (Figs. 5c and 7a–d). En echelon quartz veins and S-shaped asymmetric folds with an axial planar foliation in mylonitic schist also indicate a sinistral shear sense. However, in the Yunxian–Changning area, numerous mesoscopic upright and recumbent folds with the axes plunging gently to moderately to the south are well developed, and steeply plunging mineral lineation is locally observed on the northeasterly trending foliation. Some small-scale faults transfer into SE-SSE-trending as they merge with the Chongshan shear zone in the Mangshuijie–Xiaowan area. Such features likely suggest a subsidiary thrust component in this segment of the shear zone.

3.3. Common structural features of the shear systems

Strain distribution is heterogeneous within these shear zones within the GLSS and CSSS. The rocks within the center of the shear zone are strongly

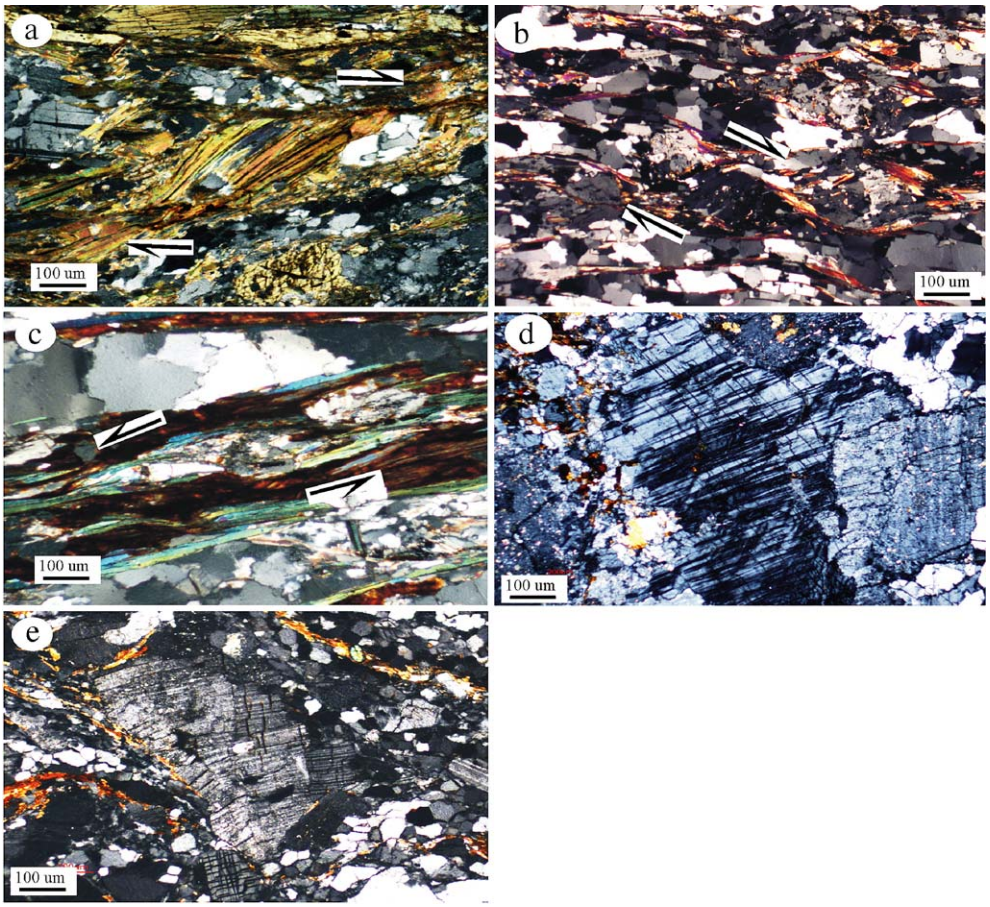

Fig. 5. (a–b) Microscopic photographs showing dextral shear sense in thin sections of 02DX-248 and 02DX-164 from the GLSS. (c) Microscopic photographs showing a sinistral shear sense in thin sections of 02DX-159 from the CSSS. (d–e) Microscopic photographs showing the kinks of twin planes in plagioclase and grain boundary migration recrystallization in thin sections of 02DX-247 and 02DX-139, respectively.

mylonitized, foliated and lineated to develop S– and S–L tectonites, and those adjacent to the margins of the shear zone show moderate mylonitization. The S-tectonites have mylonitic foliations defined by the alignment of muscovite, biotite, tabular quartz grains, pressure shadow beards and seams of opaque materials. The S–L tectonites have an additional stretching lineation that is commonly defined by elongated, preferably oriented quartz and feldspar rods, streaks of micas, and sometimes preferably oriented hornblende. The mylonitic rocks within the GLSS contain a pervasive northerly to northeasterly trending foliation with a horizontally plunging mineral lineation. In the CSSS, foliations dip moderately to steeply toward the northeast, and the stretching lineations are horizontal to shallowly plunging (Fig. 7e).

The shear senses on the GLSS and CSSS are determined on the basis of various shear-sense indicators (e.g., Cobbold et al., 1987; Twiss and Moores, 1994). The most common outcrop-scale shear sense indicators include structural lenses, asymmetrical boudins, S–C fabrics, and asymmetric porphyroblasts (Figs. 4a, d and 7a–c). On the polished surfaces of mylonitic samples that are perpendicular to foliation and parallel to lineation, S–C fabrics and asymmetric porphyroclasts are commonly present (Figs. 4b–c and 7d). A range of crystallographic-scale shear sense indicators, such as mica flakes, asymmetric porphyroblasts with recrystallized tails, S–C fabrics, antithetical microfaulted feldspar and fibrous quartz, are also extensively observed (Fig. 5a–c). Development of these asymmetric structural elements indicates a non-coaxial deformation within the shear zones (e.g., Passchier and Trouw, 1996). Such a wide range of shear sense indicators consistently indicates an intensive sinistral movement on the CSSS (Figs. 5c and 7, and Table 1) and a dextral shearing along the GLSS (Figs. 4 and 5a–b, and Table 1).

Table 1
Microscopic structural synthesis of the S–L tectonics from the Chongshan and Gaoligong shear systems

Sample	Location	Mineral assemblage	FDM	QDM	Quartz fabric	Deformation temperature	Kinematics
Chongshan shear system (CSSS)							
02DX-284	Chaojian, Yongping	Porphyroclast (~40%): Fel+Qz+Bi; matrix (~60%): Qz+Bi+Chl+Mus	CF+DC	SR+GBM	BD+RD	~350–500 °C	Sinistral
02DX-286	Wayao, Yongping	Porphyroclast (~30%): Fel+Qz+Mus+Bi; matrix (~70%): Qz+Mus+Bi+Chl	CF+DC	SR+GBM	BD+RD	~350–450 °C	Sinistral
02DX-159	Mangshuijie, Changniong	Porphyroclast (~30%): Fel+Qz+Bi; matrix (~70%): Qz+Bi+Chl	CF+DC	SR+GBM	RD	~450–550 °C	Sinistral
02DX-140	Xi'anpu, Fengqing	Porphyroclast (~40%): Fel+Qz+Bi; matrix (~60%): Qz+Bi+Chl	CF	SR+GBM	BD	~300–−400 °C	Sinistral
02DX-139	Xiawan, Fengqing	Porphyroclast (~35%): Fel+Qz+Bi; matrix (~65%): Qz+Bi+Chl	CF+DC	SR+GBM	BD+RD	~400–450 °C	Sinistral
02DX-131	Pingba, Yunxian	Porphyroclast (~40%): Fel+Qz+Bi; matrix (~60%): Qz+Bi+Chl	CF+DC	SR+GBM	BD+RD	~400–450 °C	Sinistral
02DX-126	Xiaodingxi, Yunxian	Porphyroclast (~25%): Fel+Qz+Bi; matrix (~75%): Qz+Bi+Chl	CF	SR+GBM	BD+RD	~400–450 °C	Sinistral
02DX-88	Yangtouyan, Yunxian	Porphyroclast (~35%): Fel+Qz+Bi; matrix (~65%): Qz+Bi+Chl	CF	SR+GBM	BD	~300–400 °C	Sinistral
Gaoligong shear system (GLSS)							
	Gaoligong shear zone						
02DX-246	Dahaoping, Tengchong	Porphyroclast (~20%): Fel+Qz+Bi; matrix (~80%): Qz+Bi+Chl	CF+DC	SR+GBM	RD	~400–500 °C	Dextral
02DX-247	East Dahaoping, Tengchong	Porphyroclast (~35%): Fel+Qz+Hb; matrix (~65%): Qz+Bi+Fel+Chl	Partly recrystallized feldspar grains	SR+GBM	RD	~500–550 °C	Dextral
02DX-248	Daobang, Tengchong	Porphyroclast (~30%): Fel+Qz+Bi; matrix (~70%): Qz+Bi+Chl	CF+DC	SR+GBM	BD+RD	~400–450 °C	Dextral
02DX-249	Pumanshao, Tengchong	Porphyroclast (~25%): Fel+Qz+Bi; matrix (~75%): Qz+Bi+Chl	CF+DC	SR+GBM	BD+RD	~400–450 °C	Dextral
02DX-164	Tianba, Longling	Porphyroclast (~55%): Fel+Qz++Bi; matrix (~45%): Qz+Bi+Chl	Recrystallized feldspar grains	SR+GBM	PD	~550–600 °C	Dextral
02DX-168	south Longjiang, Longling	Porphyroclast (~30%): Fel+Qz+Bi; matrix (~70%): Qz+Bi+Chl	CF+DC	SR+GBM	PD+RD	~500–600 °C	Dextral
02DX-167	West Tianba, Longling	Porphyroclast (~25%): Fel+Qz+Bi; matrix (~75%): Qz+Bi+Chl	Recrystallized feldspar grains	SR+GBM	PD	~500–600 °C	Dextral
02DX-176	Wuchalu, Luxi	Porphyroclast (~45%): Fel+Qz+Bi; matrix (~55%): Qz+Bi++Chl	CF	SR+GBM	BD	~300–400 °C	Dextral
	Nabang shear zone						
02DX-194	Nabang, Yingjiang	Porphyroclast (~35%): Fel+Hb+Qz; matrix (~65%): Qz+Fel+Bi+Chl	Partly recrystallized feldspar grains	SR+GBM	RD	~500–550 °C	Dextral
01DX-198	Pugahe, Yingjiang	Porphyroclast (~30%): Fel+Qz+Bi; matrix (~70%): Qz+Bi+Chl	CF+DC	SR+GBM	BD+RD	~300–500 °C	Dextral
02DX-203	Tongbiguan, Yinjiang	Porphyroclast (~40%): Fel+Qz+Bi; matrix (~60%): Qz+Bi+Chl	CF+DC	SR+GBM	BD+RD	~300–500 °C	Dextral

Qz: quartz; Fel: feldspar; Hb: hornblende; Mus: muscovite; Bi: biotite; Chl: chlonite; FDM: feldspar deformational mechanism; CF: cataclastic flow; DC: dislocation creep; QDM: quartz deformational mechanism; SR: rotation subgrain; GBM: grain boundary model; BD: basal <a> gliding; RD: rhombohedral gliding; PD: prism gliding.

In most mylonitic rocks within the GLSS and CSSS, quartz commonly displays crystalline-scale ductile deformation textures, and plagioclase mainly exhibits brittle deformation features (microfractures, discrete undulatory extinction, bulging and kinked twin planes; Fig. 5c–e). The deformational mechanisms of feldspar and quartz in mylonitic rocks are summarized in Table 1. Recrystallized and flattened quartz ribbons are common in these shear zones. Grain shapes of quartz are polygonal to strongly elongate. At a microscopic scale, locally developed undulatory grains with deformation bands, subgrains and serrate grain boundaries

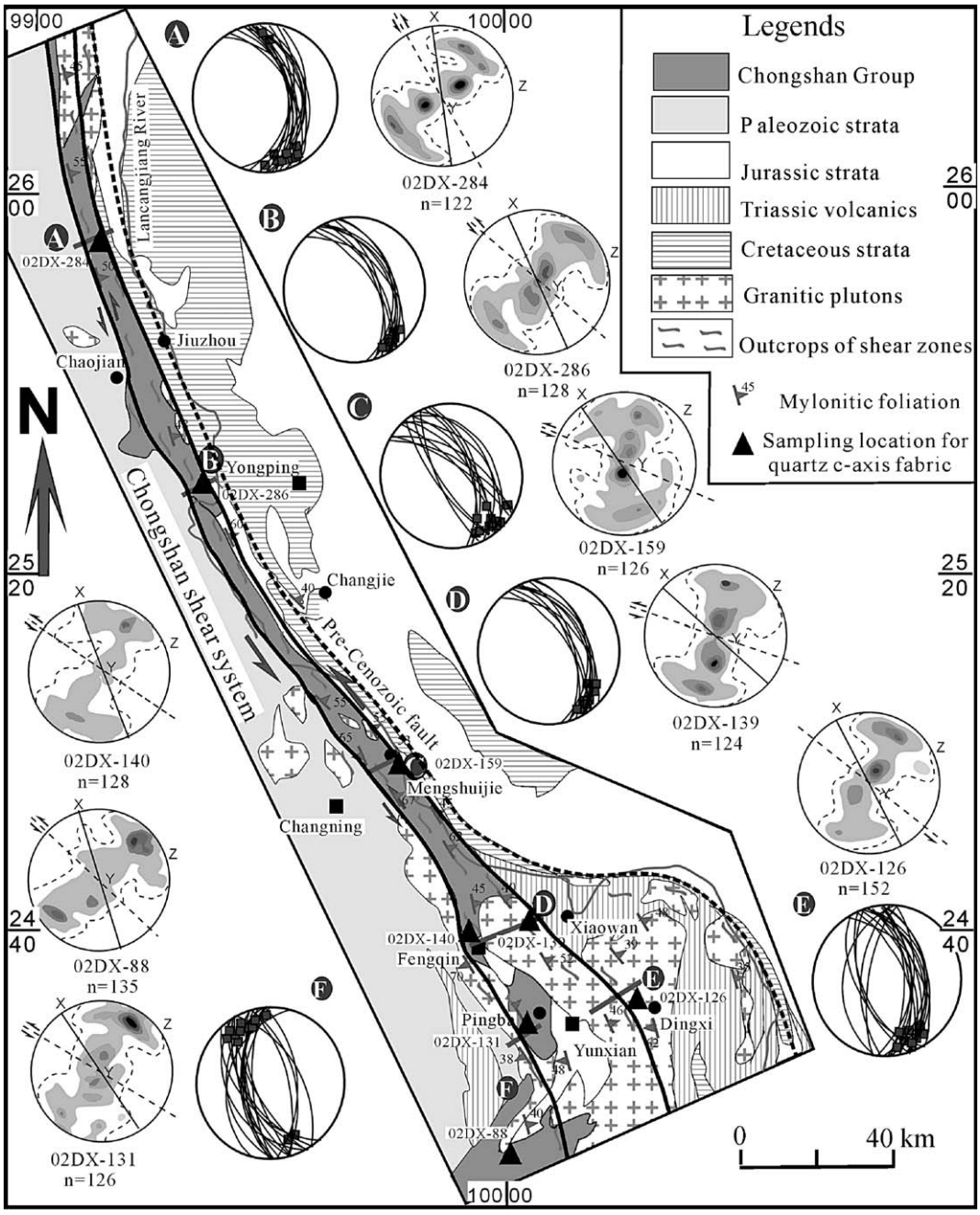

Fig. 6. Geological map of the Chongshan shear zone (CSSS) showing stereoplots (A–F) of mylonitic foliations and stretching lineations (small filled squares) and illustrations of quartz *c*-axis preferred orientations (lower hemisphere, equal area, 1%, 4%, 7% and 10% of contour intervals) for representative mylonitic samples. See Table 1 for detailed sample locations.

are indicative of quartz dislocation creep (e.g., Hirth and Tullis, 1992). Curved and kinked twin planes, and grain-scale fractures are commonly observed in feldspar from the mylonitic rocks (Fig. 5d–e). The mylonites also show recrystallized feldspar porphyroblasts with core and mantle structures. Recrystallized feldspar grains are commonly smaller than recrystallized quartz grains. Original feldspar grains form equant augen in a matrix of finely recrystallized feldspar grains. The transformation of biotite and feldspar to phyllosilicates, particularly to chlorite, sericite and muscovite is locally present, and the phyllosilicates are usually aligned

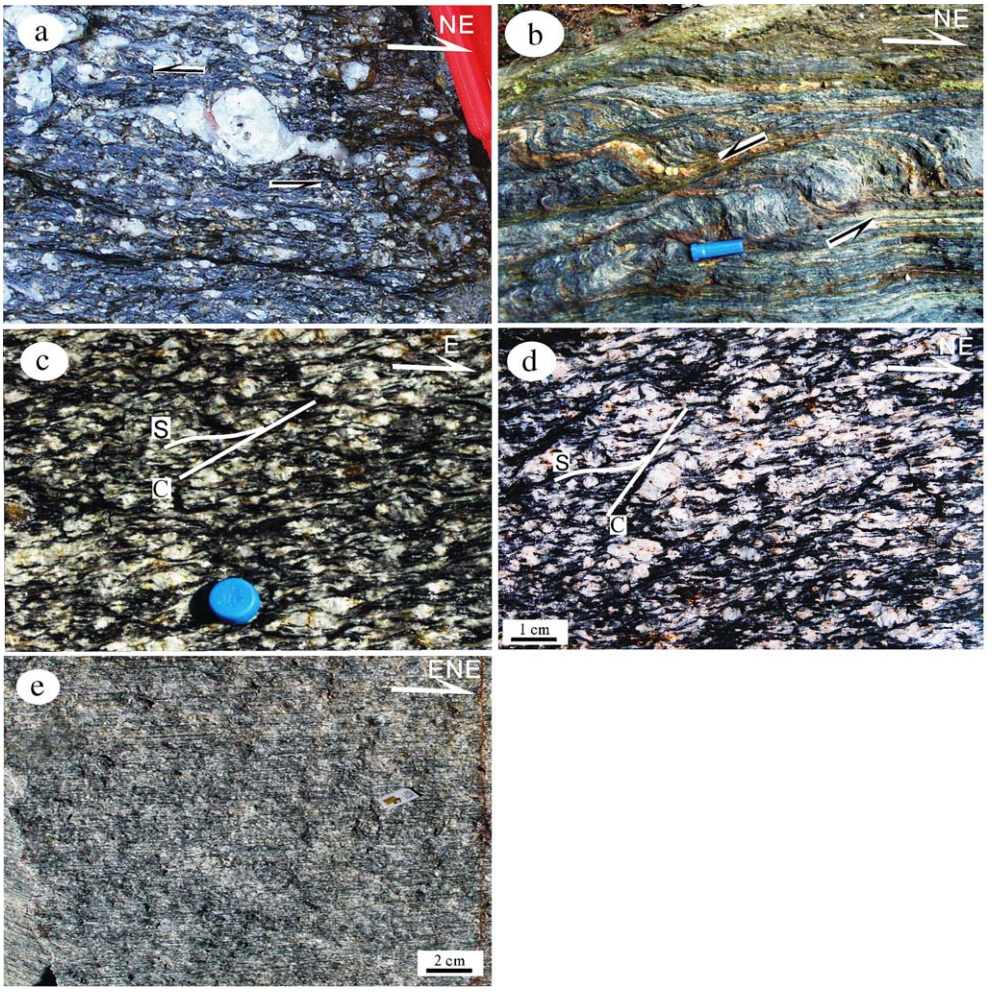

Fig. 7. Photographs showing a sinistral shear sense on the CSSS. (a) Asymmetric porphyroclasts of feldspar with strongly attenuated tails in foliated granite (Xiaowan, Fengqing), respectively. (b) Small-scale sinistral shear zones (east Changning). (c–d) S–C fabrics in foliated granitic gneisses at sites 02DX-284 and 02DX-139, respectively. (e) A prominent subhorizontally plunging mineral lineation on a northwesterly trending foliation in gneiss at site 02DX-286. (d) The polished thin section perpendicular to foliation and parallel to stretching lineation (view from above).

along the foliation, suggesting that the deformation likely continued to relatively low temperatures during the late stage of the event (Yardley, 1989). Additionally, partly recrystallized feldspar grains and hornblende porphyroblasts are present in several mylonitic samples from the GLSS (e.g., 02DX-247, 02DX-194).

3.4. Quartz c-axis fabrics

Quartz *c*-axis orientations of 19 mylonitic samples from the CSFS and GLSS have been measured using a universal stage. The locations of these samples and their quartz *c*-axis fabric patterns are illustrated in Table 1 and Figs. 3 and 6. All the quartz *c*-axis fabrics exhibit the patterns of monoclinic point-maximum asymmetry and/or maxima adjacent to *Y*-axis with respect to the foliation and lineation orientations, which can be used as a kinematic indicator (Bouchez et al., 1983; Twiss and Moores, 1994). As demonstrated in Figs. 3 and 6, these quartz *c*-axis fabric configurations are indicative of a sinistral shear sense in the CSSS and a dextral shear sense in the GLSS, consistent with other kinematic indicators described above.

The quartz *c*-axis fabric patterns of samples 02DX-176 from the GLSS (Fig. 3) and 02DX-88, -131 and -140 from the CSSS (Fig. 6) show densely populated maxima relatively near the *Z*-axis, which is probably indicative of the dominant activation of the basal <a> gliding system (Tullis et al., 1973; Law, 1990) at lower temperatures of ~350–400 °C (Tullis et al., 1973; Twiss and Moores, 1994). The patterns for samples 02DX-

164, -167 and -168 from the GLSS are characterized by *c*-axis clustering at the center (*Y*-axis) of the fabric plot, which is most likely associated with slip on the prism planes {*m*}<*a*>, a case of glide-system activation under higher temperature. The quartz *c*-axis fabric patterns of other samples, including 02DX-194, -198, -203, -246, -247, 248 and -249 from the GLSS (Fig. 3) and 02DX-139, -152, -159, -284 and 286 from the CSSS (Fig. 6), show two additional maxima close to the *Y*-axis within a broad girdle, away from the densely populated maxima relatively near the *Z*-axis. Such patterns are probably associated with slip on the rhombhedral planes {*r*}<*a*> and {*z*}<*a*>, which are normal to the *c*-axis in one of the *a* directions. This pattern is likely indicative of relatively higher temperatures during deformation, as suggested by the experimental work and polycrystal–plasticity models of Tullis et al. (1973), Tullis (1983) and Twiss and Moores (1994). All these fabric features exhibit a switching from the activation of the prism to basal gliding system for the GLSS and from rhombohedral to basal gliding for the CSSS. This means a switch from higher temperature to lower temperature crystalline gliding, consistent in the data of a thermal path from ~650 °C to ~300 °C during the deformation (Table 1). In outcrop and samples, minerals defining the high-temperature lineations often display some brittle stretching features in the same direction, suggesting that the strike-slip deformation probably continued to relatively low temperatures during late stage of the event. Therefore, based on all the data noted above and the results of previous theoretical microstructural work (e.g., Hirth and Tullis, 1992; Twiss and Moores, 1994), we infer that the deformation temperatures are in the range of ~650–300 °C for the GLSS, and ~550–300 °C for the CSSS (Table 1).

4. Mineral $^{40}Ar/^{39}Ar$ geochronology

In order to constrain the deformation age of the GLSS and CSSS and to better understand the Cenozoic tectonic evolution in the San-Jiang area, mineral separates (hornblende, muscovite and biotite) from nine mylonite samples were selected for geochronological analyses using the $^{40}Ar/^{39}Ar$ radiometric stepwise heating method (e.g., Dalrymple and Lanphere, 1971).

4.1. Analytical technique

The required mineral separates were carefully handpicked and checked under a binocular microscope; only fresh mineral concentrates of 20- to 40-mesh grain-size were selected. About 20 mg of hornblende and 10 mg of biotite were individually wrapped in Al-foil packets, encapsulated in sealed Gd-foil, and irradiated at the central thimble position of the nuclear reactor (1000 kW) at the Chinese Academy of Atomic Energy Science for 2627 min with an instantaneous neutron flux of 6.63×10^{12} n/cm^{-2}. After irradiation, the samples were progressively heated and degassed from 420 °C to 1420 °C. Purified argon was finally collected using a Zr-Al getter pump, and subsequently analyzed with a RGA-10 gas source mass-spectrometer operated in the static mode at the Institute of Geology and Geophysics, the Chinese Academy of Sciences. The analytical procedures are the same as those reported by Sang et al. (1996). Total uncertainties in each apparent age (1σ) have been calculated using the methods outlined by Dalrymple and Lanphere (1971). An internal standard biotite GA1550 (97.9±0.7 Ma) was used as a monitor to calculate the *J* value. The analytical results of mineral separates from nine representative mylonitic samples (Fig. 2) are listed in Table 2, and illustrated in Fig. 8.

4.2. Mineral $^{40}Ar/^{39}Ar$ dating results

02DX-194 is a strongly deformed plagioclase amphibolite sample from the Nabang shear zone (Nabang village, Yinjiang) and 02DX-247 is a mylonite sample from the Gaoligong shear zone (east of Dahaoping village, Tengchong), within the GLSS. In thin sections of both samples, elongated quartz ribbons and oriented muscovite and biotite flakes are present. Hornblende separates from the two samples yielded variable apparent ages during low temperature steps but well-defined plateau ages with slightly variable Ca/K ratios during intermediate-high temperature steps. The plateau ages of 32.8±0.2 Ma (02DX-194) and 32.1±0.3 Ma (02DX-247) are well defined by over 93% of ^{39}Ar gas released (Fig. 8a–b). The corresponding inverse isochron ages are consistent with their plateau ages, and the inverse ordinate intercepts are close to the $^{40}Ar/^{36}Ar$ ratio of the present-day atmosphere.

Six representative samples were collected for biotite $^{40}Ar/^{36}Ar$ analyses. Three mylonitic samples were taken from the Chongshan shear zone at Pingba (Yunxian, 02DX-131), Xiaowan (Fengqing, 02DX-139) and Mangshuijie (Changning, 02DX-159), respectively. 02DX-198 was sampled from Menggahe (Yinjiang) within the Nabang shear zone, and 02DX-164 and 02DX-249 were taken from Tianba (Longlin)

Table 2
$^{40}Ar/^{39}Ar$ isotopic analytical data for incremental heating experiments on mineral separates from the mylonites in the San-Jiang area (western Yunnan)

Temperature (°C)	$(^{40}Ar/^{39}Ar)_m$	$(^{36}Ar/^{39}Ar)_m$	$(^{37}Ar/^{39}Ar)_m$	$(^{38}Ar/^{39}Ar)_m$	$^{39}Ar_k$ (10^{-12}mol)	$(^{40}Ar/^{39}Ar_k)$ (±1 σ)	$^{39}Ar_k$ %	Apparent age (t±1 σMa)
Hornblende (Nabang, 02DX-194), weight=0.1622 g, J=0.008216								
420	38.932	0.1124	1.1489	0.1494	2.06	5.981±1.213	1.02	86.55±12.5
540	16.041	0.0511	0.8705	0.0886	3.90	1.054±0.206	1.92	15.57±3.20
660	13.568	0.0403	1.0773	0.0737	4.94	1.778±0.147	2.44	26.17±3.84
760	7.0833	0.0166	0.9083	0.0542	8.35	2.253±0.040	4.13	33.10±1.38
860	5.8163	0.0122	0.8008	0.0435	11.36	2.277±0.027	5.62	33.45±0.99
940	4.1891	0.0067	0.7552	0.0344	17.15	2.260±0.014	8.49	33.20±0.61
1020	3.8636	0.0056	0.7972	0.0311	20.40	2.254±0.012	10.1	33.11±0.56
1100	3.0000	0.0029	0.6085	0.0171	39.42	2.180±0.007	19.5	32.04±0.45
1160	2.7941	0.0021	0.6145	0.0139	55.19	2.222±0.006	27.3	32.64±0.44
1220	3.6363	0.0050	1.0929	0.0297	22.95	2.236±0.010	11.3	32.84±0.52
1320	4.8214	0.0089	1.0403	0.0383	12.98	2.277±0.019	6.42	33.44±0.74
1420	12.500	0.0357	2.8026	0.1229	3.241	2.223±0.126	1.60	32.66±4.09
Plateau age: 32.8±0.2 Ma (steps 4–11), Inverse isochron age: 31.9±0.2 Ma, $^{40}Ar/^{36}Ar$ ratio=293.6, MSWD=3.23								
Hornblende (east Dahaoping, 02DX-247); weight=0.1615g, J=0.008216								
420	30.714	0.0816	0.1238	0.1286	2.27	6.717±0.755	1.42	96.92±17.2
540	17.232	0.0547	0.1090	0.0897	3.39	1.126±0.238	2.11	16.61±3.94
660	12.245	0.0364	0.0856	0.0733	5.47	1.535±0.120	3.42	22.61±2.71
780	10.275	0.0275	0.0876	0.0572	6.73	2.168±0.084	4.20	31.86±2.70
880	7.0000	0.0163	0.0625	0.0361	11.36	2.201±0.039	7.10	32.34±1.32
960	5.9629	0.0130	0.0760	0.0340	12.52	2.154±0.028	7.83	31.66±0.97
1040	4.9210	0.0092	0.0677	0.0278	17.63	2.215±0.019	11.0	32.54±0.74
1100	4.0416	0.0062	0.0774	0.0244	22.27	2.207±0.013	13.9	32.43±0.57
1160	3.3164	0.0037	0.0800	0.0209	36.65	2.203±0.008	22.9	32.37±0.48
1220	3.3548	0.0040	0.0915	0.0245	28.76	2.174±0.009	17.9	31.94±0.48
1320	6.1666	0.0138	0.2065	0.0599	8.35	2.099±0.030	5.22	30.85±1.01
1420	9.6410	0.0256	0.1538	0.0902	4.52	2.114±0.007	2.82	31.08±2.32
Plateau age: 32.1±0.3 Ma (steps 4–11), Inverse isochron age: 32.4±0.3 Ma, $^{40}Ar/^{36}Ar$ ratio=291.2, MSWD=1.13								
Biotite (Pingba, 02DX-131), weight=0.0731g, J=0.008213								
420	12.974	0.0286	0.1209	0.0487	6.47	4.549±0.135	1.24	66.18±8.79
530	5.0375	0.0140	0.0881	0.0345	9.88	0.900±0.020	1.90	13.29±0.31
630	3.3689	0.0066	0.0584	0.0213	17.35	1.405±0.009	3.35	20.70±0.31
730	2.7743	0.0031	0.0507	0.0180	22.41	1.862±0.006	4.32	27.39±0.37
800	2.4892	0.0021	0.0403	0.1410	32.24	1.854±0.004	6.22	27.28±0.35
880	2.1090	0.0009	0.0188	0.0085	76.55	1.839±0.003	14.7	27.06±0.34
960	1.9746	0.0004	0.0194	0.0088	155.4	1.841±0.003	30.0	27.08±0.33
1040	2.0129	0.0006	0.0255	0.0103	107.8	1.822±0.003	20.8	26.80±0.33
1120	2.2910	0.0015	0.0539	0.0179	43.84	1.826±0.004	8.46	26.86±0.34
1200	2.6120	0.0025	0.0601	0.0229	26.91	1.854±0.005	5.19	27.27±0.36
1300	3.2222	0.0047	0.0937	0.0284	14.61	1.827±0.008	2.82	26.88±0.39
1400	9.2173	0.0217	0.2584	0.0918	4.27	2.847±0.068	0.82	41.71±2.87
Plateau age: 27.1±0.2 Ma (steps 4–11), Inverse isochron age: 27.0±0.3 Ma, $^{40}Ar/^{36}Ar$ ratio=296.6, MSWD=2.25								
Biotite (Xiaowang, 02DX-139), weight=0.0675g, J=0.008213								
420	10.314	0.0201	0.1222	0.0552	5.75	4.394±0.101	0.99	63.97±6.4
540	5.9793	0.0151	0.0471	0.0201	16.81	1.517±0.034	2.90	22.34±0.80
640	3.0576	0.0038	0.0396	0.0189	24.12	1.927±0.008	4.16	28.33±0.42
740	2.7375	0.0028	0.0358	0.0172	32.71	1.903±0.007	5.64	27.99±0.39
820	2.2874	0.0011	0.0183	0.0088	77.48	1.933±0.004	13.3	28.42±0.37
900	2.1258	0.0006	0.0251	0.0113	136.4	1.924±0.004	23.5	28.30±0.36
980	2.1980	0.0009	0.02816	0.0123	96.04	1.913±0.004	16.5	28.13±0.36
1060	2.3379	0.0013	0.0324	0.0162	67.27	1.932±0.005	11.6	28.41±0.37
1140	2.4017	0.0017	0.0338	0.0175	54.28	1.899±0.005	9.37	27.92±0.37

(continued on next page)

Table 2 (*continued*)

Temperature (°C)	$(^{40}Ar/^{39}Ar)_m$	$(^{36}Ar/^{39}Ar)_m$	$(^{37}Ar/^{39}Ar)_m$	$(^{38}Ar/^{39}Ar)_m$	$^{39}Ar_k$ (10^{-12}mol)	$(^{40}Ar/^{39}Ar_k)$ (±1σ)	$^{39}Ar_k$ %	Apparent age (t±1σMa)
Biotite (Xiaowang, 02DX-139), weight=0.0675g, J=0.008213								
1220	2.6582	0.0025	0.0408	0.0217	36.65	1.914±0.006	6.32	28.15±0.39
1320	2.9661	0.0033	0.0480	0.0230	27.37	1.970±0.008	4.72	28.97±0.42
1420	12.748	0.0327	0.2336	0.0945	4.24	3.127±0.155	0.73	45.75±7.01
Plateau age: 28.3±0.2 Ma (steps 3–11), Inverse isochron age: 28.2±0.2 Ma, $^{40}Ar/^{36}Ar$ ratios=298.2, MSWD=3.68								
Biotite (Mangshuijie; 02DX-159), weight=0.0722g, J=0.008216								
420	15.595	0.0382	0.2107	0.0753	5.45	4.349±0.195	1.18	63.34±12.1
520	5.8274	0.0167	0.1030	0.0339	13.17	0.914±0.027	2.87	13.50±0.40
620	4.3972	0.0095	0.0899	0.0272	18.28	1.602±0.015	3.98	23.60±0.46
700	3.4375	0.0052	0.1067	0.0252	22.27	1.912±0.009	4.85	28.12±0.43
780	2.9481	0.0037	0.0650	0.0197	31.31	1.861±0.007	6.82	27.38±0.38
860	2.4175	0.0018	0.0556	0.0114	63.33	1.880±0.004	13.8	27.66±0.35
940	2.2200	0.0011	0.0417	0.0123	104.3	1.893±0.003	22.7	27.85±0.35
1020	2.3003	0.0015	0.0532	0.0152	72.61	1.832±0.004	15.8	26.95±0.34
1100	2.2702	0.0013	0.0471	0.0133	85.83	1.873±0.004	18.7	27.56±0.35
1200	3.1355	0.0042	0.1097	0.0284	27.37	1.896±0.008	5.96	27.89±0.40
1300	4.7843	0.0098	0.1832	0.0525	11.83	1.915±0.018	2.57	28.18±0.62
1400	14.608	0.0434	0.6362	0.1783	2.67	1.881±0.172	0.58	27.68±4.73
Plateau age: 27.6±0.3 Ma (steps 4–11), Inverse isochron age: 27.5±0.4 Ma, $^{40}Ar/^{36}Ar$ ratio=295.0, MSWD=6.76								
Biotite (Menggahe, 02DX-198), weight=0.0668g, J=0.008194								
420	12.236	0.0255	0.1260	0.0773	7.26	4.731±0.120	1.31	68.62±8.12
520	6.8275	0.0205	0.0901	0.0569	11.29	0.795±0.037	2.04	11.72±0.46
620	4.5431	0.0107	0.0585	0.0371	18.28	1.374±0.016	3.31	20.20±0.41
700	3.2678	0.0044	0.0458	0.0305	25.98	1.957±0.008	4.71	28.70±0.42
780	2.8437	0.0031	0.0339	0.0221	37.11	1.925±0.006	6.73	28.24±0.38
860	2.2527	0.0013	0.0177	0.0113	84.44	1.847±0.004	15.3	28.10±0.34
940	2.1739	0.0008	0.0174	0.0103	133.3	1.916±0.003	24.1	28.11±0.35
1020	2.3043	0.0010	0.0197	0.0116	106.7	1.983±0.004	19.3	29.08±0.37
1100	2.3958	0.0017	0.0291	0.0163	66.81	1.884±0.004	12.1	27.65±0.35
1200	2.7428	0.0028	0.0391	0.0225	40.59	1.903±0.006	7.36	27.92±0.37
1300	4.1515	0.0075	0.0890	0.0519	15.31	1.931±0.014	2.77	28.32±0.53
1400	10.111	0.0277	0.2604	0.1406	4.18	1.969±0.082	0.76	28.89±2.40
Plateau age: 28.1±0.2 Ma (steps 4–11), Inverse isochron age: 28.0±0.2 Ma, $^{40}Ar/^{36}Ar$ ratio=296.5, MSWD=14.46								
Biotite (Tianba; 02DX-164), weight=0.0614g, J=0.008194								
420	14.163	0.0300	0.1358	0.0566	5.41	5.337±0.161	1.27	77.22±12.2
520	7.4330	0.0223	0.0771	0.0333	10.39	0.872±0.044	2.46	12.84±0.59
620	4.8860	0.0116	0.0531	0.0205	18.32	1.462±0.019	4.33	21.49±0.48
700	3.3631	0.0049	0.0446	0.0171	23.31	1.900±0.009	5.52	27.88±0.42
780	2.9256	0.0033	0.0357	0.0157	34.33	1.932±0.006	8.12	28.34±0.39
860	2.3888	0.0013	0.0228	0.0098	83.51	1.979±0.004	19.7	28.02±0.37
940	2.1565	0.0008	0.0218	0.0137	133.3	1.899±0.003	31.5	27.87±0.35
1020	2.4800	0.0020	0.0423	0.0252	57.99	1.893±0.003	13.7	27.78±0.36
1100	3.3725	0.0049	0.0815	0.0323	23.66	1.936±0.005	5.60	28.40±0.43
1200	3.8441	0.0064	0.0793	0.0318	17.86	1.939±0.012	4.22	28.44±0.48
1300	5.1777	0.0111	0.1161	0.0439	10.43	1.918±0.021	2.47	28.14±0.69
1400	11.062	0.0313	0.2391	0.0868	3.71	1.892±0.098	0.88	27.76±2.73
Plateau age: 28.2±0.3 Ma (steps 4–11), Inverse isochron age: 28.3±0.3 Ma, $^{40}Ar/^{36}Ar$ ratio=293.0, MSWD=8.14								
Biotite (Pumanshao, 02DX-249), weight=0.0642g, J=0.008213								
420	9.1560	0.0159	0.1163	0.0401	7.28	4.480±0.067	1.23	65.20±4.37
540	5.4805	0.0142	0.0583	0.0177	17.86	1.280±0.024	3.01	18.87±0.50
640	3.1153	0.0038	0.0441	0.0127	30.15	1.984±0.007	5.09	29.17±0.41
740	2.6190	0.0023	0.0328	0.0092	48.71	1.918±0.005	8.23	28.20±0.37
820	2.3055	0.0013	0.0304	0.0071	83.51	1.896±0.004	14.1	27.84±0.35
900	2.1911	0.0007	0.0269	0.0055	157.7	1.973±0.003	26.6	29.01±0.36

Table 2 (*continued*)

Temperature (°C)	$(^{40}Ar/^{39}Ar)_m$	$(^{36}Ar/^{39}Ar)_m$	$(^{37}Ar/^{39}Ar)_m$	$(^{38}Ar/^{39}Ar)_m$	$^{39}Ar_k$ (10^{-12}mol)	$(^{40}Ar/^{39}Ar_k)$ (±1 σ)	$^{39}Ar_k$ %	Apparent age (t±1 σMa)
Biotite (Pumanshao, 02DX-249), weight=0.0642 g, J=0.008213								
980	2.3139	0.0011	0.0400	0.0080	99.75	1.971±0.004	16.8	28.98±0.37
1060	2.4193	0.0016	0.0488	0.0104	71.91	1.945±0.004	12.1	28.60±0.37
1140	2.9655	0.0034	0.0899	0.0203	33.63	1.956±0.004	5.68	28.75±0.40
1220	3.2608	0.0043	0.0953	0.0239	26.67	1.987±0.008	4.50	28.21±0.43
1320	5.2222	0.0111	0.1740	0.0522	10.43	1.968±0.022	1.76	28.93±0.73
1420	16.047	0.0449	0.4188	0.1060	3.87	2.875±0.206	0.65	42.11±8.60
Plateau age: 28.4±0.2 Ma (steps 3–11), Inverse isochron age: 28.6±0.3 Ma, $^{40}Ar/^{36}Ar$ ratio=297.0, MSWD=9.61								
Muscovite (Xûyi; 02DX-51), *weight=0.0653 g, J=0.008194*								
420	16.682	0.0384	0.1961	0.1029	4.82	5.389±0.223	1.45	77.97±17.0
540	10.486	0.0324	0.1907	0.0627	8.58	0.962±0.088	2.59	14.17±1.26
640	8.2176	0.0225	0.1427	0.0457	12.36	1.605±0.054	3.74	23.58±1.30
740	3.8202	0.0056	0.0904	0.0329	20.64	2.173±0.011	6.24	31.85±0.53
820	3.0000	0.0031	0.0592	0.0209	37.11	2.083±0.007	11.2	30.54±0.43
900	2.5405	0.0013	0.0429	0.0128	85.83	2.143±0.005	25.9	31.41±0.41
980	2.8181	0.0022	0.0606	0.0170	51.03	2.152±0.006	15.4	31.54±0.43
1060	2.9189	0.0027	0.0685	0.0232	42.91	2.127±0.006	12.9	31.18±0.43
1140	3.3467	0.0040	0.0907	0.0310	28.76	2.166±0.009	8.70	31.75±0.48
1220	3.6800	0.0049	0.1036	0.0351	23.19	2.216±0.011	7.01	32.48±0.53
1320	5.3260	0.0108	0.1966	0.0510	10.67	2.145±0.023	3.22	31.43±0.81
1420	9.6410	0.0256	0.3787	0.0733	4.52	2.130±0.007	1.36	31.23±2.34
Plateau age: 31.5±0.2 Ma (steps 3–12), Inverse isochron age: 31.4±0.1 Ma, $^{40}Ar/^{36}Ar$ ratio=294.6, MSWD=6.66								

Notes: parameter $\lambda=5.543e^{-10}$/a; $(^{40}Ar/^{39}Ar)_m$: measured values of $^{40}Ar/^{39}Ar$; $^{39}Ar_k$: measured values of $^{39}Ar_k$ which was produced by *k* decay. MSWD: mean square of the weight deviates.

and Pumanshao (Tengchong) within the Gaoligong shear zone, respectively. All these samples exhibit extensive mylonitic foliation and stretching lineation, and contain preferably aligned quartz ribbons, preferably oriented feldspar and mica flakes. Biotites occur as small grains outlining the stretching lineation and within shear planes. The biotite separates from the six samples yielded well-defined plateau ages during intermediate-high temperature-heating steps (Fig. 8c–h). The corresponding plateau ages are 27.1±0.2 Ma (02DX-131), 28.3±0.2 Ma (02DX-139), 27.6±0.3 Ma (02DX-159), 28.1±0.2 Ma (02DX-198), 28.2±0.3 Ma (02DX-164) and 28.4±0.2 Ma (02DX-249), respectively. These ages are defined by more than 92% of total ^{39}Ar release, and their $^{40}Ar/^{36}Ar$ initial ratios (293–298) are consistent with the present atmospheric $^{40}Ar/^{36}Ar$ ratio (295.5).

Synkinematic muscovite separates are from a mylonitic sample (02DX-51) at Xûyi (Shuangjiang), south of Yunxian (Fig. 2). The sample contains a northwesterly dipping foliation with a shallowly plunging mineral lineation, and exhibits a sinistral shear sense (Chen et al., 2006). The separates yielded a $^{40}Ar/^{39}Ar$ plateau age of 31.7±0.2 Ma with 92% of ^{39}Ar released during the continuously nine temperature-heating steps (Fig. 8i).

5. Discussion

5.1. Shearing timing of the shear systems

In most cases, the $^{40}Ar/^{39}Ar$ ages represent the mineral cooling ages. However, if the deformation temperature is near to the closure temperature of $^{40}Ar/^{39}Ar$ isotopic system of mineral separates, the $^{40}Ar/^{39}Ar$ plateau ages may record the timing of synkinematic mineral crystallization (Kirschner et al., 1996). Accepting that the argon closure temperatures of biotites, muscovites and hornblendes (Dodson, 1973; Harrison et al., 1985; Hames and Bowring, 1994) are 320±40 °C, 450±50 °C and 510±50 °C, respectively, and also taking into account the aforementioned shearing conditions (Table 1), the $^{40}Ar/^{39}Ar$ plateau ages of 32–33 Ma (early Oligocene) for hornblende separates (02DX-194 and-247) and 32 Ma for muscovites separates (02DX-51) likely date the shearing movement along the dextral GLSS and sinistral CSSS, respectively. We also note that: (1) Eocene strata are involved in the Wuliangshan arcuate structure; and (2) middle Eocene strata exhibit consistent deformation patterns with the older rocks, and upper Oligocene strata unconformably overlay the folded pre-Eocene sequence in the southern Lanping–Simao fold belt, south of the CSSS (BGMRYP, 1990; Wang and Burchfiel, 1997,

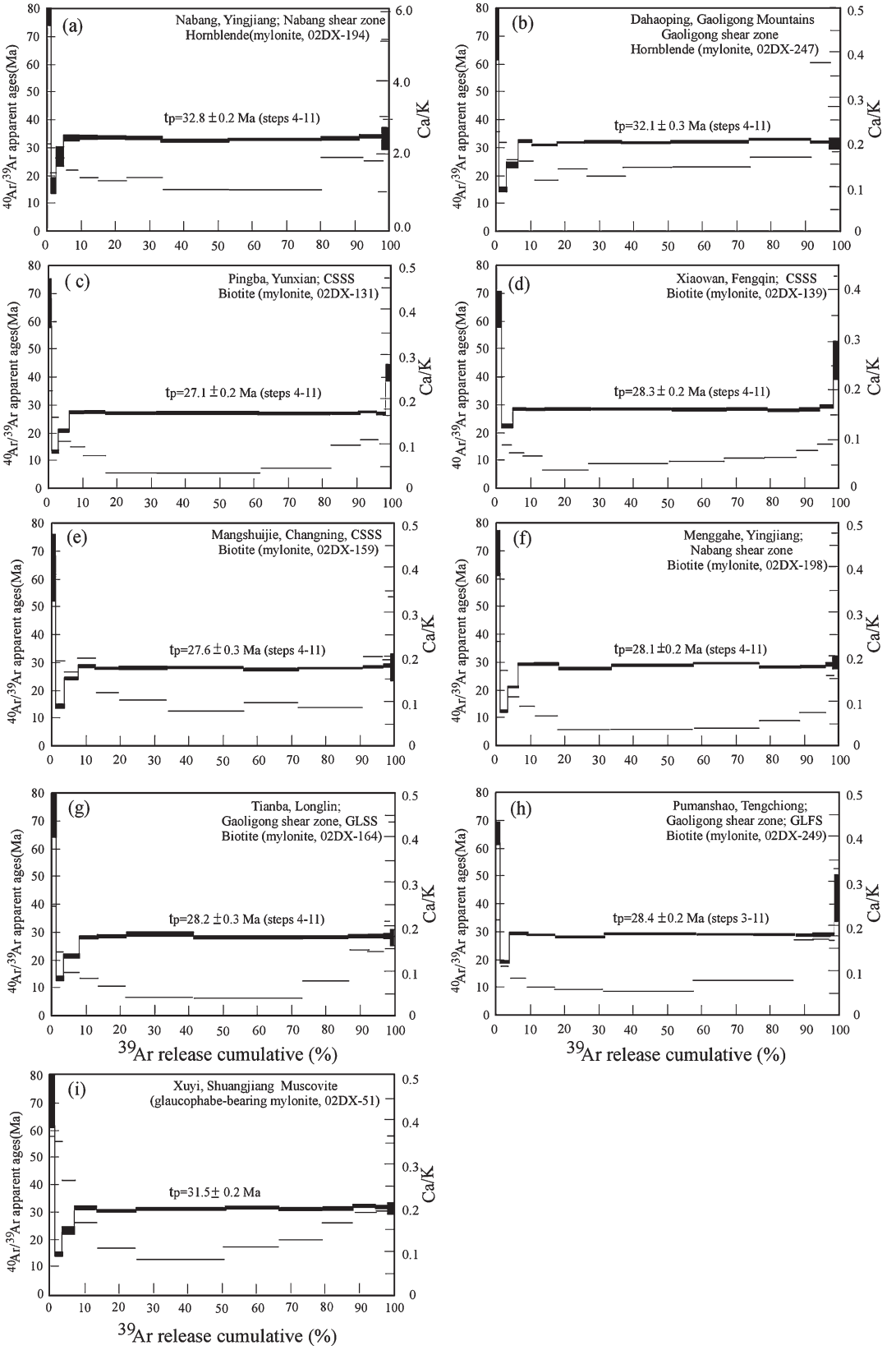
(a)
Nabang, Yingjiang; Nabang shear zone
Hornblende(mylonite, 02DX-194)
tp=32.8 ±0.2 Ma (steps 4-11)
(b)
Dahaoping, Gaoligong Mountains
Gaoligong shear zone
Hornblende (mylonite, 02DX-247)
tp=32.1 ± 0.3 Ma (steps 4-11)
(c)
Pingba, Yunxian; CSSS
Biotite (mylonite, 02DX-131)
tp=27.1 ±0.2 Ma (steps 4-11)
(d)
Xiaowan, Fengqin; CSSS
Biotite (mylonite, 02DX-139)
tp=28.3 ± 0.2 Ma (steps 4-11)
(e)
Mangshuijie, Changning, CSSS
Biotite (mylonite, 02DX-159)
tp=27.6 ± 0.3 Ma (steps 4-11)
(f)
Menggahe, Yingjiang;
Nabang shear zone
Biotite (mylonite, 02DX-198)
tp=28.1 ±0.2 Ma (steps 4-11)
(g)
Tianba, Longlin;
Gaoligong shear zone, GLSS
Biotite (mylonite, 02DX-164)
tp=28.2 ±0.3 Ma (steps 4-11)
(h)
Pumanshao, Tengchiong;
Gaoligong shear zone; GLFS
Biotite (mylonite, 02DX-249)
tp=28.4 ±0.2 Ma (steps 3-11)
(i)
Xuyi, Shuangjiang Muscovite
(glaucophabe-bearing mylonite, 02DX-51)
tp=31.5± 0.2 Ma
$^{40}Ar/^{39}Ar$ apparent ages(Ma)
Ca/K
^{39}Ar release cumulative (%)

2000). These geological observations indicate that the shearing timing of the shear systems mainly occurred before late Oligocene, consistent with our $^{40}Ar/^{39}Ar$ geochronological results of synkinematic minerals. The $^{40}Ar/^{39}Ar$ plateau ages of 27–29 Ma for biotite separates date the cooling event through argon closure temperature following the synkinematic growth of biotite. As noted above, the lowest temperature of the shearing deformation for both the GLSS and CSSS is inferred to be 300~350 °C, thus the age of 27–29 Ma might define time of the late-stage shearing on the GLSS and CSSS.

Lacassin et al. (1997) reported that development of the sinistral WCSZ and TPSZ, which are subparallel to the ASRRSS and sliced the middle part of the Indochina Block (see Fig. 1), at least began at 33–36 Ma and possibly terminated at ~29 Ma, coeval with the shearing history of the GLSS and CSSS. The recently geochronological data showed that the monazite inclusions from garnets cores to rimes in mylonitic paragneisses along the ASRRSS yielded Th–Pb ages of 30–34 Ma (Gilley et al., 2003). Some felsic igneous rocks along the ASRRSS, which might be the anatexic products in response to the shearing heating, gave U–Pb zircon ages of >32 Ma (Schärer et al., 1994; Leloup et al., 1995; Zhang and Schärer, 1999; Leloup et al., 2001; Wang et al., 2001). These ages were interpreted to document the onset time of shearing motion along the ASRRSS (Gilley et al., 2003). Matrix monazite, reflective of protracted high-temperature metamorphism during shearing along the ASRRSS, was dated at 28–19 Ma with a majority cluster of 28–25 Ma (Gilley et al., 2003). Published $^{40}Ar/^{39}Ar$ ages of synkinematic biotites, which might document the ages of late-stage shearing along the ASSRSS, mainly vary from 26 Ma to 17 Ma (e.g., Leloup et al., 1995; Wang et al., 1998, 2000; Leloup et al., 2001). Therefore, sinistral movement on the ASRRSS mainly occurred at 28–17 Ma, but was initiated before ~32 Ma.

In summary, our structural analyses and all the available geochronological data of synkinematic minerals clearly indicate that the major shear systems in SE Asia (e.g., GLSS, CSSS, ASRRSS, WCSZ and TPSZ) might have a similar onset age of >32 Ma (early Oligocene), coeval with the initial seafloor spreading in the South China Sea as constrained by the magnetic anomalies (~32 Ma, Briais et al., 1983), although the age of late-stage shearing on these shear zones are different (27–29 Ma for the GLSS, CSSS and WCSZ and ~17 Ma for the ASRRSS).

5.2. Implications for the tectonic extrusion of SE Asia

Lacassin et al. (1997) concluded that the WCSZ that separated the Southern Indochina Block from the Northern Indochina Block, was a sinistral strike-slip shear zone developed during early Oligocene. Previous data show that the WCSZ extends through the southeastern Tibetan syntaxis not far away from north of the Zangbo suture (Tapponnier et al., 1986; Armijo et al., 1989), and probably join with the Nyainqengthangta shear zone (Replumaz and Tapponnier, 2003). Although the southward continuation of the CSSS is poorly constrained, a series of shear zones illustrated by BGMRYP (1990) along the southern Lancangjiang granitic pluton (south of Yunxian) show the signatures of sinistral shearing (Chen et al., 2006) and gave a shearing age of ~32 Ma at Xûyi (02DX-51). These seem to suggest that the southward continuation of the CSSS is overprinted by early Oligocene sinistral strike-slip shearing, and have similar kinematics and shearing history to the CSSS, WCSZ and ASRRSS. In contrast to the CSSS, the GLSS was a dextral strike-slip shear system during early Oligocene. Therefore, dextral movement on the GLSS was contemporaneous with sinistral movement on the CSSS, ASRRSS and WCSZ during early Oligocene. Taking into account that the dextral Sagaing fault was not active prior to 15 Ma (Morley et al., 2001; Replumaz and Tapponnier, 2003), we consider that the Baoshan and Southern Indochina Blocks likely had an affinity to the Yangtze craton, and the Tengchong and Burma Blocks were part of the India plate during early Oligocene. At the time, the western boundary of the Indochina extrusion Block in SE Asia might be the dextral Gaoligong shear zone in the GLSS (Leloup et al., 1995; Replumaz and Tapponnier, 2003), rather than the Sagaing fault as proposed by Tapponnier et al. (1986, 1990).

The geophysical data show that, during ~30–40 Ma, the India plate was rotated anticlockwisely with a rotation angle of −7.7°, and the Southern Indochina Block was rotated clockwisely with rotation angle of 9.6°, faster than the rotation of the North Indochina Block (e.g., Patriat and Achache, 1984; Replumaz and Tapponnier, 2003). Incorporating with the other data

Fig. 8. $^{40}Ar/^{39}Ar$ apparent ages and Ca/K spectra of hornblende and biotite separates from mylonite samples. Coarse lines give the apparent ages (the length of bars notes 1σ uncertainty), while fine lines show Ca/K ratios. (a) Hornblende, 02DX-194; (b) hornblende, 02DX-247; (c) biotite, 02DX-131; (d) biotite, 02DX-139; (e) biotite, 02DX-159; (f) biotite, 02DX-198; (g) biotite, 02DX-164; (h) biotite, 02DX-249; (i) muscovite, 02DX51. See Fig. 2 for sample locations.

from previous studies (e.g., Schärer et al., 1994; Leloup et al., 1995; Lacassin et al., 1997; Zhang and Schärer, 1999; Wang et al., 2000; Leloup et al., 2001; Morley et al., 2001; Gilley et al., 2003; Lee et al., 2003; Replumaz and Tapponnier, 2003), we here propose the following scenario for the Tertiary tectonic extrusion of the SE Asia. During early Oligocene period, since the India plate moved the north obliquely toward the Eurasia plate, the Tengchong and Burma Blocks, as parts of the triangular indentation zone north of the India plate, dextrally moved northward along the GLSS. Accompanying with the northward motion, the Northern Indochina Block extruded toward the southeast along the ASRRSS and CSSS, and the Baoshan/Southern Indochina Blocks along the CSSS and Gaoligong shear zone, respectively. As discussed above, the late-stage shearing (also corresponding to rapid cooling) is dated at ~27–29 Ma on the GLSS, CSSS and WCSZ and ~17 Ma on the ASRRSS (e.g., Leloup et al., 2001). After the time, the shearing deformation in these shear systems probably terminated and the subsequent deformation was dominated by the development of numerous brittle faults. Our synthesis above indicates that the main extrusion of the Northern Indochina Block along the ASRRSS lasted longer than that of the Baoshan/Southern Indochina Blocks along the CSSS. This is different to the general expectation that the shearing extrusion period of the Northern Indochina block along the ASRRSS should be similar to or even shorter than that of the Baoshan/Southern Indochina block, as their extrusion escaping rates are probably similar and the former more directly faced the impinging syntaxis of the India plate than the latter. A more likely scenario is that the Baoshan/Southern Indochina block may have rotationally escaped southeastward along the CSSS to the east and the GLSS to the west faster than the Northern Indochina block between the ASRRSS and CSSS during early Oligocene. Until ~27–29 Ma, the Baoshan block was likely relatively away from the impinging syntaxis and likely had a decreasing rate of tectonic extrusion. By contrast, the Northern Indochina block was closer to the impinging syntaxis and exhibited rapid and more intensive extrusion.

Following this reasoning above, the CSSS may have been changed from ductile transpression to brittle transtension deformation during 28–17 Ma, similar to that of the WCSZ. The extension induced the development of the normal faults and resulted in the denudation and rapid cooling of the footwall of the fault zone. During this period, the ASRRSS became the largest discontinuity in SE Asia and continued sinistral strike-slip shearing (Leloup et al., 1993, 1995; Dunning et al., 1995; Lacassin et al., 1997; Wang and Burchfiel, 1997; Wang et al., 1998, 2000; Leloup et al., 2001; Lee et al., 2003), accommodating further southeastward extrusion. As a result, the Northern Indochina Block was continuously extruded along the ASRRSS relative to the South China Block.

6. Conclusions

A new kinematic and $^{40}Ar/^{39}Ar$ geochronological study on the Gaoligong and Chongshan shear systems (GLSS and CSSS), western Yunnan, China allows us to reach the following conclusions:

(1) The CSSS is a sinistral strike-slip shear system and the GLSS is a dextral strike-slip shear system, both are developed under amphibolite- to greenschist-grade conditions.
(2) The $^{40}Ar/^{39}Ar$ dating of synkinematic hornblende, muscovite and biotite on the CSSS and GLSS yielded the $^{40}Ar/^{39}Ar$ plateau ages of ~32 Ma and 27–29 Ma, respectively. The CSSS and GLSS have a similar shearing onset time to the ASRRSS and WCSZ (early Oligocene) but different shearing termination time (27–29 Ma on the GLSS, CSSS and WCSZ and ~17 Ma on the ASRRSS). The strike-slip shearing on major shear systems in SE Asia was contemporaneous with seafloor spreading in the South China Sea (~32–17 Ma).
(3) During early Oligocene (27–36 Ma), the western boundary of the Indochina extrusion Block might be the dextral Gaoligong shear zone rather than the Sagaing fault. The Baoshan/Southern Indochina Block was clockwisely extruded southeastward along the CSSS and GLSS faster than the Northern Indochina Block along the ASRRSS, accompanying with obliquely northward motion of the India plate.

Acknowledgements

We are grateful to Prof. Bin Xia for helpful discussions. She-Fa Chen, Jean-Pierre Burg and an anonymous reviewer are thanked for their critical and constructive review, which led to major improvement of the manuscript. Financial support for this study was jointly provided by the Ministry of Science and Technology of China (2002CB412603), National Nature Sciences Foundation of China (40334039, 40421303 and 40473019), the Chinese Academy of

Science (KZCX2-SW-117), the Wang K-C Education Foundation (Hong Kong).

References

Armijo, R., Tapponnier, P., Mercier, J.L., Tonglin, H., 1989. Late Cenozoic right-lateral strike-slip faulting in southern Tibet. J. Geophys. Res. 94, 2787–2838.

BGMRYP (Bureau of geology and mineral resources of Yunnan Province), 1990. Regional Geology of Yunnan Province. Geological Publishing House, Beijing.

Bouchez, J.L., Lister, G.S., Nicoals, N., 1983. Fabric asymmetry and shear sense in movement zones. Geol. Rundsch. 72, 401–420.

Briais, A., Patriat, P., Tapponnier, P., 1983. Updated interpretation of magnetic anomalies and seafloor spreading stages in the South China Sea, implications for the Tertiary tectonics of SE Asia. J. Geophys. Res. 98, 6299–6328.

Cattin, R., Avouac, J.P., 2000. Modeling mountain building and the seismic cycle in the Himalaya of Nepal. J. Geophys. Res. 105 (13), 389–407.

Chen, X.Y., Wang, Y.J., Fan, W.M., Peng, T.P., 2006. The microstructure characteristics of Chongshan–Lincang Shear Zones in Yunnan Province and its tectonic signification. Geotecton. Metallogen. 30 (1), 41–51.

Cobbold, P., Gapais, D., Means, W.D., Treagus, S.H., 1987. Shear criteria in rocks. J. Struct. Geol. 9, 1–778.

Dalrymple, G.B., Lanphere, M.A., 1971. $^{40}Ar/^{39}Ar$ technique of K/Ar dating: a comparison with the conventional technique. Earth Planet. Sci. Lett. 12, 300–308.

Dewey, J.F., Cande, S., Pitman, W.C.I., 1989. Tectonic evolution of the India/Eurasia collision zone. Eclogae Geol. Helv. 82, 717–734.

Dodson, M.H., 1973. Closure temperature in cooling geochronological and petrological systems. Contrib. Mineral. Petrol. 40, 259–274.

Dunning, G.R., Macdonald, A.S., Barr, S.M., 1995. Zircon and monazite U–Pb dating of the Doi Inthanon core complex, northern Thailand: implications for extension within the Indosinian orogen. Tectonophysics 251, 197–213.

England, P., Houseman, G., 1989. Finite strain calculation of continental deformation: 2. Comparison with the India–Asia collision zone. J. Geophys. Res. 91, 3664–3676.

England, P., Molnar, P., 1990. Right-lateral shear and rotation as the explanation for strike-slip faulting in eastern Tibet. Nature 344, 140–142.

Gilley, L.D., Harrison, T.M., Leloup, P.H., Ryerson, F.J., Lovera, O. M., Wang, J.H., 2003. Direct dating of left-lateral deformation along Red River shear zone, China and Vietnam. J. Geophys. Res. 108 (B2), 2127.

Hames, W.E., Bowring, S.A., 1994. An empirical evaluation of the argon diffusion geometry in muscovite. Earth Planet. Sci. Lett. 124, 161–167.

Harrison, T.M., Duncan, I., McDougall, L., 1985. Diffusion of ^{40}Ar in biotite: temperature, pressure and compositional effects. Geochim. Cosmochim. Acta 49, 2261–2468.

Hirth, G., Tullis, J., 1992. Dislocation creep regimes in quartz aggregates. J. Struct. Geol. 14, 144–159.

Houseman, G., England, P., 1993. Crustal thickening versus lateral expulsion in the India–Asian continental collision. J. Geophys. Res. 98, 12233–12249.

Ji, J.Q., Zhong, D.L., Sang, H.Q., Zhang, L.S., 2000. The western boundary of extrusion blocks in the southeastern Tibetan Plateau. Chin. Sci. Bull. 45 (10), 870–875.

Kirschner, L., Cosca, M.A., Masson, H., Hunziker, J.C., 1996. Staircase $^{40}Ar/^{39}Ar$ spectra of fine-grained white mica: timing and duration of deformation and empirical constraints on argon diffusion. Geology 24 (8), 747–750.

Lacassin, R., Maluski, H., Leloup, H., Tapponnier, P., Hinthong, C., Siribhakdi, K., Chuaviroj, S., Charoenravat, A., 1997. Tertiary diachronic extrusion and deformation of western Indochina: structural and $^{40}Ar/^{39}Ar$ evidence from NW Thailand. J. Geophys. Res. 102 (B5), 10013–10037.

Law, R.O., 1990. Crystallographic fabrics: a selective review of their applications to research in structural geology. In: Knipe, R.J., Rutter, E.H. (Eds.), Deformation Mechanism, Rheology and Tectonics. Geol. Soc. Spec. Pub., vol. 54, pp. 335–352.

Lee, H.Y., Chung, S.L., Wang, J.R., Wen, D.J., Lo, C.H., Yang, T.Y., Xie, Y.W., Lee, T.Y., Wu, G.Y., Ji, J.Q., 2003. Miocene Jiali faulting and its implications for Tibetan tectonic evolution. Earth Planet. Sci. Lett. 205, 185–194.

Leloup, P.H., Kienast, J.R., 1993. High temperature metamorphism in a major Tertiary ductile strike-slip shear zone: the Ailaoshan–Red River (P.R.C.). Earth Planet. Sci. Lett. 118, 213–234.

Leloup, P.H., Harrison, T.M., Ryerson, F.J., Chen, W., Qi, L., Tapponnier, P., Lacassin, R., 1993. Structural, petrological and thermal evolution of a Tertiary ductile strike-slip shear zone, Diancangshan, Yunnan. J. Geophys. Res. 98, 6715–6743.

Leloup, P.H., Lacassin, R., Tapponnier, P., Zhong, D., Liu, X., Zhang, L., Ji, S., Trinh, P.T., 1995. The Ailao Shan–Red River shear zone (Yunnan, China), Tertiary transform boundary of Indochina. Tectonophysics 251, 3–84.

Leloup, P.H., Arnaud, N., Lacassin, R., Kienast, J.R., Harrison, T.M., Phan Trong, T.T., Replumaz, A., Tapponnier, T., 2001. New constraints on the structure, thermochronology, and timing of the Ailao Shan–Red River shear zone, SE Asia. J. Geophys. Res. 106, 6683–6732.

Liu, Z., Li, X., Ye, Q., Lou, J., Shen, G., 1993. Division of Tectono-Magmatic Zones and the Distribution of Deposits in the Sanjiang Area. Geol. Publ. House, Beijing. (in Chinese with English abstract).

Meyer, B., Tapponnier, P., Bourjot, L., Metivier, F., Gaudemer, Y., Peltzer, G., Guo, S.M., Chen, Z.T., 1998. Crustal thickening in Gansu–Qinghai, lithospheric mantle subduction, and oblique, strike-slip controlled growth of the Tibet Plateau. Geophys. J. Int. 135, 1–47.

Mitchell, A.H.G., 1993. Cretaceous–Cenozoic tectonic events in the west Myanmar (Burma)–Assam region. J. Geol. Soc. (Lond.) 50, 1089–1102.

Morley, C.K., Woganan, N., Sankumarn, N., Hoon, T.B., Alief, A., Simmons, M., 2001. Late Oligocene–Recent stress evolution in rift basins of Northern and Central Thailand: implications for escape tectonics. Tectonophysics 334, 115–150.

Passchier, C.W., Trouw, R.A.J., 1996. Microtectonics. Springer. 289 pp.

Patriat, P., Achache, J., 1984. India–Eurasia collision chronology has implications for crustal shortening and driving mechanism of plates. Nature 311, 615–621.

Pelzer, G., Tapponnier, P., 1988. Formation and evolution of strike-slip faults, rifts, and basins during the India–Asia collision: an experimental approach. J. Geophys. Res. 93, 15085–15117.

Peng, T.P., Wang, Y.J., Fan, W.M., Liu, D.Y., Shi, Y.R., Miao, L.C., 2006. The SHRIMP zircon U–Pb geochronology of the early

Mesozoic felsic igneous rocks from the southern Lancangjiang and its tectonic implications. Sci. China (D Series) 36 (2), 123–132.

Replumaz, A., Tapponnier, P., 2003. Reconstruction of the deformed collision zone between India and Asia by backward motion of lithospheric blocks. J. Geophys. Res. 108 (B6), 2285, doi:10.1029/2001JB000661.

Sang, H.Q., Wang, S.S., Qiu, J., 1996. The ^{40}Ar-^{39}Ar ages of pyroxene, hornblende and plagioclase in Taipingzhai granulites in Qianxi County, Hebei Province and their geological implications. Acta Petrol Sin 12 (4), 390–400 (in Chinese with English abstract).

Schärer, U., Zhang, L., Tapponnier, P., 1994. Duration of strike-slip movements in large shear zones: the Red River belt, China. Earth Planet. Sci. Lett. 126, 379–397.

Tapponnier, P., Peltzer, G., Armijo, R., Le Dain, A.Y., Cobbold, P., 1982. Propagating extrusion tectonics in Asia: new insights from simple experiments with plasticine. Geology 10, 611–616.

Tapponnier, P., Peltzer, G., Armijo, R., 1986. On the mechanics of the collision between India and Asia. In: Coward, M.P., Ries, A.C. (Eds.), Collision Tectonics. Geol. Soc. Spec. Publ., vol. 19, pp. 115–157.

Tapponnier, P., Lacassin, R., Leloup, H., Schärer, U., Zhong, D., Liu, X., Ji, S., Zhang, L., Zhong, J., 1990. The Ailao Shan–Red River metamorphic belt: Tertiary left-lateral shear between Indochina and South China. Nature 343, 431–437.

Tullis, J., 1983. Deformation of feldspars. In: Ribbe, P.H. (Ed.), Feldspar Mineralogy. Mineralogical Society of America, pp. 297–323.

Tullis, J., Christie, J.M., Griggs, D.T., 1973. Microstructure and preferred orientations of experimentally deformed quartzite. Geol. Soc. Amer. Bull. 84, 297–314.

Twiss, R.J., Moores, E.M., 1994. Structural Geology. W.H. Freeman and Company, New York, pp. 215–422.

Wang, Y., 1983. The characteristics and significance of Carboniferous gravel beds in the Tengchong and Baoshan area, western Yunnan. In: Zhou, Z., Xu, X., Zhou, W. (Eds.), Geology of Qinghai–Xizang (Tibet) Plateau, Beijing, vol. 11, pp. 71–77.

Wang, E.C., Burchfiel, B.C., 1997. Interpretation of Cenozoic tectonics in the right-lateral accommodation zone between the Ailaoshan shear zone and the eastern Himalayan syntaxis. Int. Geol. Rev. 39, 191–219.

Wang, E.C., Burchfiel, B.C., 2000. Late Cenozoic to Holocene deformation in southwestern Sichuan and adjacent Yunnan, China, and its role in formation of the southeastern part of the Tibetan Plateau. GSA Bull. 112 (3), 413–423.

Wang, P.L., Lo, C.H., Lee, T.Y., Chung, S.L., Lan, C.Y., Yem, N.T., 1998. Thermochronological evidence for the movement of the Ailao Shan–Red River Shear Zone: a perspective from Vietnam. Geology 26, 887–890.

Wang, P.L., Lo, C.H., Chung, S.L., Lee, T.Y., Lan, C.Y., Thang, T.Y., 2000. Onset timing of left-lateral movement along the Ailao Shan–Red River shear zone: ^{40}Ar/^{39}Ar dating constraint from the Nam Dinh area, northeastern Vietnam. J. Asian Earth Sci. 18, 281–292.

Wang, J.H., Yin, A., Harrison, T.M., Grove, M., Zhang, Y.Q., Xie, G. H., 2001. A tectonic model for Cenozoic igneous activities in the eastern Indo-Asian collision zone. Earth Planet. Sci. Lett. 188, 123–133.

Yardley, B.W.D., 1989. An Introduction to Metamorphic Petrology. Logman Group UK Ltd, London.

Zhang, L.S., Schärer, U., 1999. Age and origin of magmatism along the Cenozoic Red River shear belt, China. Contrib. Mineral. Petrol. 134, 67–85.

Zhong, D.L., 1998. Paleotethyan Orogenic Belts in Yunnan and Western Sichuan. Science Press, Beijing. 230 pp.